



Analyst

Accepted Manuscript

This article can be cited before page numbers have been issued, to do this please use: J. Albahri, D. Smaje, Y. Xu, S. Robinson, H. Allison, K. A. Whitehead and H. Muhamadali, *Analyst*, 2025, DOI: 10.1039/D5AN00507H.



This is an Accepted Manuscript, which has been through the Royal Society of Chemistry peer review process and has been accepted for publication.

Accepted Manuscripts are published online shortly after acceptance, before technical editing, formatting and proof reading. Using this free service, authors can make their results available to the community, in citable form, before we publish the edited article. We will replace this Accepted Manuscript with the edited and formatted Advance Article as soon as it is available.

You can find more information about Accepted Manuscripts in the <u>Information for Authors</u>.

Please note that technical editing may introduce minor changes to the text and/or graphics, which may alter content. The journal's standard <u>Terms & Conditions</u> and the <u>Ethical guidelines</u> still apply. In no event shall the Royal Society of Chemistry be held responsible for any errors or omissions in this Accepted Manuscript or any consequences arising from the use of any information it contains.



3 4

57

58 59

60

View Article Online DOI: 10.1039/D5AN00507H

Metabolic Fingerprinting of Periodontal Bacteria: A Multi-scale Mass Spectrometry and Vibrational Spectroscopy Approach

Jawaher Albahri^{1,2}, Daniel Samje¹, Yun Xu¹, Steven Robinson³, Heather Allison⁵, Kathryn A. Whitehead⁴, Howbeer Muhamadali¹ *

- 1- Centre for Metabolomics Research, Department of Biochemistry, Cell and Systems Biology, Institute of Systems, Molecular and Integrative Biology, University of Liverpool, Liverpool L69 7ZB, UK
- Department of Pharmaceutical Chemistry, College of Pharmacy, King Khalid University, Abha 62529, Saudi Arabia
- 3- Materials Innovation Factory, University of Liverpool, Liverpool L7 3NY, UK
- 4- Microbiology at Interfaces, Department of Life Sciences, Manchester Metropolitan University, Chester St, Manchester M1 5GD, UK
- 5- Department of Clinical Infection, Microbiology, and Immunology. Institute of Infection, Veterinary and Ecological Sciences, University of Liverpool, Liverpool, L69 7ZB, UK

Corresponding authors *:

Howbeer Muhamadali, Email: Howbeer.muhamad-ali@liverpool.ac.uk

Abstract

Periodontitis is a prevalent condition characterised by progressive destruction of the supporting periodontium around teeth, resulting from prolonged interaction between the host immune system and bacterial infection. Classifying periodontal bacteria remains challenging due to their high diversity, culturability, strain level variability, biofilm complexity, and methodological constraints. Fourier Transform Infrared (FT-IR) spectroscopy was employed to investigate the biochemical composition of five oral Streptococcus spp., Porphyromonas gingivalis, Actinomyces israelii, Fusobacterium nucleatum, and Parvimonas micra at microbial-community level. In parallel, Matrix-Assisted Laser Desorption/Ionisation Time-of-Flight (MALDI-TOF) mass spectrometry, the gold standard analytical platform in clinical settings, was used for a comprehensive understanding of cellular protein/peptide molecules, identifying approximately 20 m/z values associated with the clustering pattern. Particularly, P. gingivalis was distinctly clustered within higher m/z range (8000-16500), primarily driven by features at 9329, 9800, and 11029 m/z, highlighting the potential of this window for its specific identification. Additionally, Optical Photothermal Infrared (O-PTIR) spectroscopy, combined with chemometrics, was also utilised at single-cell level. Classification patterns across IR techniques and MALDI-MS were comparable, revealing significant variation in protein and lipid profiles among the studied strains. P. gingivalis, F. nucleatum, A. israelii exhibited distinct clustering, while S. anginosus and S. oralis showed significant variation within the Streptococcus spp. The overall clustering pattern was primarily attributed to spectral information within amides (1500-1800 cm⁻¹) and fatty acids (2800-3050 cm⁻¹) regions, alongside vibrational bands observed between (900-1200 cm⁻¹), indicative of polysaccharides and phosphate-containing compounds. The submicron spatial resolution demonstrated by O-PTIR, suggests promising potential for direct application to clinical samples without the need for prolonged culturing.

54

55

56 57

58

59

60

1

Keywords: FT-IR spectroscopy; O-PTIR spectroscopy; MALDI-TOF-MS; fingerpring ricce Online periodontitis.

Introduction

Periodontitis is a globally pervasive condition characterised by the progressive inflammation of the periodontal tissues, resulting from a complex interaction between microbial infection and the host immune response (1). Nevertheless, the progression of periodontitis is contingent upon dysbiotic alterations in the oral microbiome in response to the breakdown products of periodontal tissues and the efficacy of anti-bacterial mechanisms (2). According to the complex theory, oral bacteria associated with subgingival plaque formation are classified into five colour-labelled groups based on their presence in tooth colonisation and periodontitis severity (3). The red complex bacteria Porphyromonas gingivalis, Tanerrela forsythia, and Treponema denticola are known as the keystone pathogens in chronic periodontitis, they are strict anaerobes and late colonisers in subgingival biofilm formation, appearing in later stages of periodontitis (4). Clinically, impacts of periodontitis are not restricted to the oral cavity. As it has been explored in our previous review (5), periodontal pathogens and their toxins can disseminate to distal parts of the body, having been reported in conjunction with some systemic diseases such as Alzheimer's disease (6), Parkinson's disease (7), chronic kidney disease (8), and diabetes (9), highlighting its broader clinical relevance. Beyond oral health, periodontitis imposes economic burden, with global costs, including treatment expenses and productivity loss, estimated to be in the billions annually (10).

The application of appropriate detection and identification methods provides valuable information on the early diagnosis of periodontitis, assisting in designing preventive and therapeutic intervention strategies, which have been demonstrated by recent studies (11, 12). Although the traditional microbial phenotyping methods including Gram staining, microscopy tests, colony morphology, and analytical profile index (API) tests are still valuable, they are often time-consuming, subjective, have specificity limitations and struggling to differentiate closely related species (13). Many methods require up to 48 hours to acquire reliable results for these fastidious bacteria (14). Such methods require complementary techniques for fast, precise, and reliable results. Vibrational spectroscopy and mass spectrometry techniques, as metabolic fingerprinting approaches, have attracted a lot of interest for such applications. These approaches are generally quick and reproducible, requiring minimal sample preparation, with the potential to provide simultaneous information on a diverse range of biomolecules, including lipids, proteins, nucleotides, and carbohydrates (15, 16).

Fourier Transform Infrared (FT-IR) spectroscopy, in particular, has been widely used for bacterial identification and classification (17-19). In this technique, the absorption of IR light by distinct functional groups induces changes in bond vibrations involving stretching or bending, consequently causing specific variations in the dipole moment (20). The resultant distinctive spectral profile displays unique characteristics, forming a metabolic fingerprint, which can be utilised for the identification or discrimination of samples, as has been reported previously (21,

46

47 48

49

50

51 52

53

54

55 56

57

58

59 60 22). FT-IR has been extensively utilised across various fields, such as the pharmaceutical industry victe Online (23, 24), clinical diagnostics (25, 26), and even environmental research (27). However, the diffraction limit of FT-IR restricts its application to bulk measurements, requiring large cell clusters for sufficient signal (28-30). Optical Photothermal Infrared (O-PTIR) spectroscopy, on the other hand, is a novel vibrational technique providing IR measurements and contactless imaging with the superior advantage of providing sub-micron spatial resolution in comparison to traditional FT-IR microscopy. It has excellent spectral sensitivity and the ability to collect highquality spectra within a very short time with minimal sample preparation required (31). Such characteristics have facilitated the exploration of numerous metabolomics investigations at the single-cell level, such as human cellular specimen differentiation (32), bacterial cell discrimination (33), and detection of antimicrobial resistance in bacteria (34). In contrast to FT-IR spectroscopy, the capabilities of O-PTIR are constrained to the measurement of infrared spectra exclusively within the fingerprint region (950-1800 cm⁻¹). This limitation arises from the coverage of the utilised quantum cascade laser (QCL), which selectively covers this specific spectral range (18). However, recent advancements in new O-PTIR platforms have integrated QCL with tuneable Optical Parametric Oscillator (OPO) lasers, providing continuous tunability across a wider range of wavelengths (35).

On the other hand, Matrix-Assisted Laser Desorption Ionisation Mass Spectrometry (MALDI-MS) is a well-established technique that has been widely used for bacterial identification and discrimination at the microbial community level (36, 37). It is a soft ionisation technique in which a laser induces ionisation of bacterial samples with the assistance of the appropriate matrix, such as sinapinic acid (SA), α -cyano-4-hydroxycinnamic acid (HCCA), or 2,5-dihydroxybenzoic acid (DHB) (38). The generated molecular ions then travel inside the Time Of Flight (TOF) mass analyser, where they separately reach the detector based on their mass-to-charge ratio (m/z) (39). In contrast to the vibrational spectroscopic techniques, MALDI-TOF-MS spectral results provide information mainly about the protein and peptide content within the bacterial cells (40). For bacterial identification, the generated protein profile could then be matched to reference profiles stored in organism-specific databases (41). The reproducibility, speed and ease of sample preparation have made MALDI-TOF-MS the gold-standard analytical technique for bacterial identification in clinical settings, through platforms such as Bruker's Biotyper.

In the present study, *P. gingivalis*, a representative of the red complex pathogens, alongside, eight strains representatives of the other microbial complexes also investigated. Facultative anaerobes *Streptococcus anginosus*, *Streptococcus constellatus*, *Streptococcus gordonii*, *Streptococcus sanguinis*, and *Streptococcus oralis*, and three obligate anaerobes including *Actinomyces israelii*, *Fusobacterium nucleatum*, and *Parvimonas micra*. Thus, our primary objective is to conduct a fingerprint analysis to characterise the selected nine periodontal bacteria employing mid-infrared spectroscopy in addition to comparison with MALDI-TOF-MS as the gold standard analytical platform in clinical settings and for more holistic information about cellular protein/peptide molecules. To the best of our knowledge, this study marks the first characterisation of the selected bacteria combining FT-IR, and O-PTIR spectroscopic methodologies in addition to MALDI-TOF-MS. This pioneering approach is designed to comprehensively investigate the biochemical composition of these bacterial strains at both the microbial community and single-cell levels.

4 5

6 7

8

9 10

11

12

13 14

Pan Access Article, Publishe don 42 November 4023, Downloaded on 44. 1, 2023 L7:55: 19.

45 46

47

48

49

50 51

52

53

54 55

56

57

58 59

60

View Article Online DOI: 10.1039/D5AN00507H

Growth conditions and sample preparation

S. anginosus (NCTC 11169), S. constellatus (NCTC 11063), S. gordonii (NCTC 7870), S. sanguinis (NCTC 10904), S. oralis (NCTC 11427), A. israelii (NCTC 6831), F. nucleatum (NCTC 10562), P. gingivalis (NCTC 11834), and P. micra (NCTC 11808) were purchased from National Collection of Type Cultures (NCTC) in lyophilised form and aseptically reconstituted and cultured following their instructions and recommended growth conditions. In order to eliminate any potential bias and changes in metabolic fingerprints of the cells associated with the components of different culturing media, fastidious anaerobic agar (Neugen culture media, UK) supplemented with 5% defibrinated horse blood (TCS Biosciences, UK) was used as a control growth medium to support the growth of all nine strains in this study. All culture plates were kept in an anaerobic chamber for 24 h before use. The strains were subcultured anaerobically three times to achieve axenic colonies. A single colony was streaked to make three biological replicates for the FT-IR analysis and five biological replicates for MALDI-TOF-MS analysis. The plates were anaerobically incubated at 37 °C for 24 h for the five Streptococcus spp., 48 h for P. micra, 72 h for A. israelii and F. nucleatum, and a week for P. gingivalis using OxoidTM anaerobic jars. The anaerobic atmosphere inside the jars was frequently checked using OxoidTM Resazurin Anaerobic Indicator.

FT-IR spectroscopic analysis

Samples were prepared following the established pipeline used in our previous work, which yielded spectra within the linear range (17, 34). Bacterial biomass was collected from the blood agar plate using a 10 μL inoculation loop (Sigma-Aldrich, UK) and resuspended in 1 mL of sterile physiological saline solution (0.9% NaCl). The optical density of the bacterial slurries was recorded at 600 nm wavelength (OD_{600nm}) using a 6705 UV/Vis spectrophotometer (Jenway, UK). The samples were then centrifuged and washed using the sterile saline solution twice at a temperature of 4 °C and a speed of 5000 g for 6 min to remove the supernatant and any residuals from the culture media. After the final washing step, the supernatant was removed, and the bacterial pellets were kept for further analysis. Samples were randomised using Microsoft Excel's random number generation function to ensure unbiased allocation. All samples were normalised on the same day to an OD_{600nm} of 20 using sterile saline solution, before spotting 20 µL of each onto an FT-IR silicon plate (Bruker Ltd., UK), which was thoroughly washed and dried as previously outlined (42). The plate was left to dry overnight in a desiccator and then placed in a 50 °C oven for 45 min before performing the FT-IR analysis. FT-IR spectral data were collected in absorbance mode within the mid-infrared region (600-4000 cm⁻¹), with 4 cm⁻¹ spectral resolution, using a Bruker Invenio FTIR spectrometer (Bruker Ltd., UK). In total, 12 spectra were obtained for each strain, resulting from three biological replicates and four technical replicates to provide a representative of the microbial population and detect any variations in terms of sample heterogeneity. FT-IR data collection was conducted via OPUS spectroscopy software (Bruker Ltd., UK). All spectral data were pre-processed following the optimised workflow reported in our previous studies (17, 36, 43). Since the instrument is not N₂ purged, the atmospheric CO₂ effect was removed by replacing the CO₂ vibrations (2400 - 2275 cm⁻¹) with a linear trend. Then, the

Ther 2025 Downloaded for 14. 10. 2025 17:55: 10. Creative Commons. Attribution 3.0 Unported Licence

spectra were scaled using the extended multiplicative signal correction method (EMSC) to reduce online the variation attributed to the scattering effect before performing data analysis (44).

MALDI-TOF-MS analysis

Sample preparation optimisation

Sinapinic acid (Sigma Aldrich, UK) was used as the matrix, and mixing method was employed for sample deposition. Sample preparation was optimised to identify the most appropriate amount of bacterial biomass to provide decent peaks with acceptable reproducibility and signal-to-noise ratio. *Escherichia coli* MG1655 was used to optimise the sample preparation method. Bacterial cultures were prepared following the methods described in the growth condition section above. The bacterial biomass was then carefully collected using a sterile 20 μ L plastic loop and resuspended into 1 mL of deionised (DI) water, which was vortexed until it became homogenous, then 100 μ L was used to measure the OD₆₀₀ using a 6705 UV/Vis spectrophotometer (Jenway, UK), while the remaining sample was washed twice using DI water as described above. All bacterial pellets were then stored at -80 °C freezer until further analysis. The optimisation investigated twelve different conditions, including four different normalised ODs ranging from the lowest value of OD_{600nm} of 5 up to 20. In parallel, three different ratios of sample to the matrix were tested, including mixing equal volumes (1:1), doubling the sample volume (2:1), and doubling the matrix volume (1:2).

Periodontal bacterial samples

In total, five biological replicates were prepared and stored at – $80\,^{\circ}$ C freezer until further analysis. The defrosted pellets were then normalised to OD_{600nm} of 10 (optimal bacterial load) using DI water containing 0.1% trifluoroacetic acid (TFA). The matrix was prepared by dissolving 10 mg of sinapinic acid in 500 μ L of acetonitrile and 500 μ L of water containing 2% TFA. An aliquot (20 μ L) from the normalised bacterial sample was then mixed with 20 μ L of the matrix and vortexed for 20 s. Randomisation of samples was performed using Microsoft Excel by generating random numbers and subsequently sorting the samples based on these values to ensure unbiased distribution. Then, 2 μ L of the bacterial mixture was spotted on a microtiter plate 384-well polished steel plate (Bruker Ltd., UK) and left to dry at room temperature for 1 h.

Samples were then analysed using a Bruker Autoflex Speed time-of-flight mass spectrometer equipped with a Bruker smartbeamTM-II laser (355 nm wavelength). The instrument was operated in positive ion mode, and linear TOF was used over the range from 1000 to 80,000 *m/z*. The full-width at half maximum (FWHM) for representative peaks at low, medium, and high ends within the *m/z* range containing detectable peaks 2000 to 17000 *m/z* (**Table S1**). Each sample had five biological replicates, and from each biological replicate, five analytical replicates were prepared. The results of this analysis generated 225 MALDI-TOF-MS spectra: 9 bacteria x 5 biological replicates x 5 technical replicates. The instrument was calibrated using five standard proteins (MSCAL3) from Sigma Aldrich, UK including (molecular weight provided in parentheses) insulin (5630), cytochrome c (12,185), apomyoglobin (16,722), aldolase (39,212), and albumin (66,430). A mixture of the five proteins was prepared as per the supplier's recommendation. Then aliquots (2 μL) of the (1:1) sinapinic acid: standards mixture were spotted

58

59

60

1 2

3

after every five samples on the plate. Mass accuracy achieved after calibration was calculated hoosooth using (**Equation1**) (45). That included the standards covering the range (2000-1700 m/z) (**Figure S1**) giving an overall average error around 168 ppm (**Table S2**), which is within the accepted mass error tolerance in peptide mass fingerprinting (46). MS data were collected using Bruker flexAnalysis software. All MS spectra were baseline corrected, then subjected to morphological score correction and filtered using signal-to-noise ratio threshold of 10, followed by vector normalisation.

Equation1

Mass error (ppm) =
$$\left| \frac{m_{measured} - m_{reference}}{m_{reference}} \right| \times 10^6$$

O-PTIR single-cell analysis

Samples were prepared by taking 100 µL aliquots of the bacterial slurries from the FT-IR samples and diluted with 900 µL of DI water. The samples were then centrifuged and washed twice with DI water at 4°C and 5000 g for 6 min before undergoing serial dilution with DI water to achieve a single-cell distribution of the sample. Aliquots of 2 µL of each sample were then spotted on a calcium fluoride (CaF₂) slide in a descending order from the highest to the lowest concentration to determine the best dilution at which we can achieve single bacterial cells. The samples were then dried in a 50 °C oven for 30 min before carrying out the O-PTIR analysis. Single-point O-PTIR spectra of up to 55 individual bacterial cells from each sample spot were collected in the reflection mode within the mid-infrared region (950-1800 cm⁻¹, and 2 cm⁻¹ spectral resolution) through Schwarzschild objective (40×, 0.78 NA) using a mIRage microscope (Photothermal Spectroscopy Corp., Santa Barbara, CA, USA), equipped with tunable quantum cascade laser (QCL) and a continuous-wave (CW) 532 nm laser, which act as pump and probe beams, respectively. Single-frequency images were obtained by tuning the QCL to vibrational modes associated with amide I at (1655 cm⁻¹) and polysaccharides at (1061 cm⁻¹). Probe power was adjusted to 39% with an imaging pixel size of 0.2 µm and a settle time of 10 min. O-PTIR data were filtered by removing all the vibrational bands with intensities below 0.1 at the amide I peak (1655 cm⁻¹), resulting in a final five to eight spectra for each strain coming from different single cells, the resulted spectra were then subjected to gaussian smoothing using a window size of 20 data points and autoscaled.

Multivariate statistical analysis

Data processing and analysis were carried out using MATLAB® (version r2024a, The MathWorks Inc., UK). All data were subjected to the Principal Component Analysis (PCA), an unsupervised method used to minimise the dimensionality of the multivariate data while retaining most of its variability without prior knowledge of samples classification in the dataset (47, 48). Then, a supervised method of Principal Component-Discriminant Function Analysis (PC-DFA) was employed to analyse the data. In this method, DFA is applied to principal components (PCs) to find linear combinations that best discriminate between predefined classes (48). However, PC-DFA was used as a semi-supervised method following the similar approach applied in our

48 49

50

51

52

53 54

55

56

57 58

59

60

previous study (17), where the algorithm was provided only with information regarding the provided only with the provided only wi

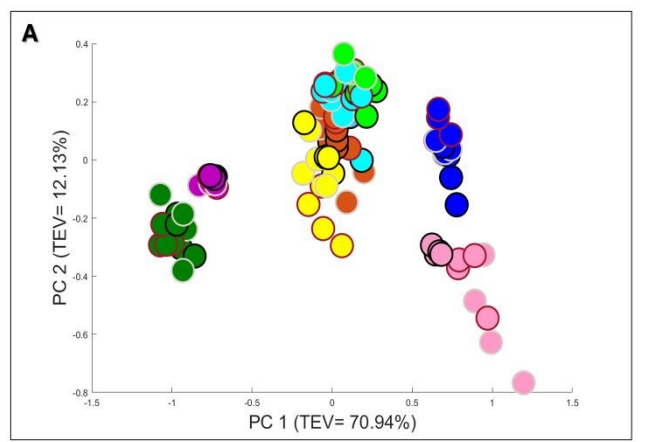
Results and discussion

Discrimination at microbial-community level

FT-IR fingerprint analysis

Infrared spectra of all nine periodontal microorganisms were collected using FT-IR spectroscopy to investigate the variance in their biochemical composition in the bulk population. The results of FT-IR analysis showed that the variance between the samples displayed variation in the three main regions of the IR spectra, including fingerprint (900-1200 cm⁻¹), amides (1500-1700 cm⁻¹), and lipids (2800-3000 cm⁻¹) regions (**Figure S2**, and **S3**). The PCA scores plot of the FT-IR spectral data collected from these samples displayed four distinct clusters according to PC1 and PC2 axes, with a combined total explained variance (TEV) of 83.1% (Figure 1A). The clustering patterns observed was different to Socransky's complex theory (3), which classified subgingival bacteria based on DNA hybridisation profiles. While Socransky's model groups P. gingivalis and F. nucleatum, into the red and orange complexes, respectively, in the present study, these two species were clustered closely together on the negative side of PC1 accounting for 70.94% of the TEV in the dataset. A. israelii, belonging to the blue complex, was postioned on the positive side of PC1 axis. S. sanguinis, S. gordonii, and S. oralis, which are all from the yellow complex, were found clustered in the middle together, as expected. The clustering pattern of the three isolates is consistent with their assignment to the Streptococcus mitis group, as members of this group reliably form well-defined clusters in both gene-based and whole-genome phylogenetic analyses (49, 50). Such clustering supports the conclusion that the isolates share a common genetic background characteristic of the mitis group. However, two other strains from the orange complex, S. constellatus and P. micra were clustered with bacteria from the yellow complex. Furthermore, S. anginosus was distinctly separated on PC1 from the other Streptpcoccus spp.. These differences likely reflect the distinct biological features captured by FT-IR biochemical profiling compared to DNA-based association patterns. While the PCA is an unsupervised approach, the results showed tight clustering of the data within the same class, emphasising the high reproducibility of the FT-IR results. According to the PC1 loadings plot, accounting for 70.94% of the TEV, vibrational bands attributed to polysaccharides due to C-O stretching at 1061 cm⁻¹ influence the separation of S. anginosus and A. israelii on the positive side of the PC1 axis. In contrast, the spectral features that significantly contributed to the discrimination of P. gingivalis and F. nucleatum along the negative axis of PC1, include the following main vibrations: the amide I at 1634 cm⁻¹ and amide II at 1543 cm⁻¹, attributed to C=O stretching and N-H bending coupled with C-N stretching, respectively. Moreover, fatty acids vibrational bands at 2961 cm⁻¹ of C-H asymmetric stretching, and 2920, and 2851 cm⁻¹ assigned to C-H asymmetric, and symmetric stretching of the methylene group, respectively (Figure 1B). Since the samples are mixed-species, the corresponding loading plots reflects variations in the overall biochemical composition of the bacterial cells, separation occurring along PC axes based on differences in general biomolecular features. Due the observed variation among the Streptococcus strains, and to further investigate

the variation at the species level, the FT-IR dataset of the *Streptococcus spp.* was separately in analysed detailed in a later section. Furthermore, since all the nine strains were grown on fastidious anaerobic agar (FAA) supplemented with 5% defibrinated horse blood, another FT-IR fingerprint analysis was performed where the samples were grown on different media as per the supplier recommendation and using the same media as control FAA with 5% defibrinated horse blood as control (**Figure S4**). The results showed a similar clustering pattern across all conditions, indicating that the observed clustering is attributable to phenotypic differences rather than background-dependent effects.



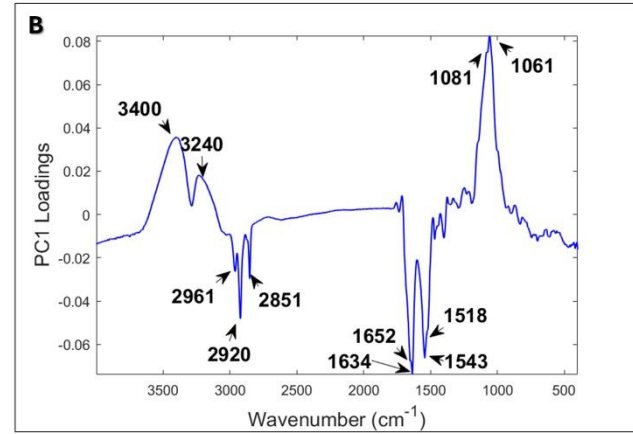


Figure 1 (**A**) shows PCA score plot obtained using processed FT-IR data of the nine periodontal bacteria cultured under the same growth conditions using fastidious anaerobic agar supplemented with 5% horse defibrinated blood. Key colours used in figures: *S. anginosus* (•), *S. constellatus* (•), *S. gordonii* (•), *S. oralis* (•), *S. sanguinis* (•), *P. micra* (•), *A. israelii* (•), *F. nucleatum* (•), and *P. gingivalis* (•). Different outline colours represent different biological replicates. (**B**) represents PC1 loadings of FT-IR spectral data including fatty acids region (2800-3050 cm⁻¹), amides region (1500-1800 cm⁻¹), mixed region (1250-1450 cm⁻¹), polysaccharides region (900-1200 cm⁻¹), and fingerprint region (600-900 cm⁻¹).

MALDI-TOF-MS analysis

MALDI is a soft ionisation technique which has been widely used for proteins measurements in bacterial cells (38). Since there is no universal matrix or standard technique for the deposition of sample/matrix mixture, the MALDI-TOF-MS sample analysis protocols were tested using E. coli MG1655 as a representative strain for method optimisation. To optimise MALDI-TOF-MS spectral quality and ensure reproducibility through evaluating bacterial concentrations normalised by optical density (OD_{600}) across a range of 5 to 20. This range was selected to examine the influence of cell density on ionisation efficiency and signal-to-noise ratio. At lower ODs (e.g., 5), the protein content was insufficient for reliable detection, whereas very high ODs (e.g., 20) led to matrix suppression and ion suppression effects, resulting in inconsistent signal intensities and peak distortion (**Figure S5**, **S6**, and **S7**). Empirical assessment identified an intermediate OD_{600} of 10 as optimal, providing sufficient protein mass for consistent ionisation while minimising suppression artefacts. This normalisation produced reproducible, high-intensity MALDI-TOF-MS profiles, enabling robust and accurate comparative analyses between samples. The results showed that the spectral data collected from samples with OD_{600nm} of 10 using a mixing ratio of 1:1 was the most reproducible method, with a relative error of 22-33% (**Table S3**). These findings

53

54

55 56

57

58

59 60 are in agreement with the literature since the mixing ratio of 1:1 is the most frequently applied No0507H ratio in several MALDI-TOF-MS studies for bacterial characterisation (36, 51). The optimised method was used as the standard approach to characterise the periodontal bacteria at microbial community level using MALDI-TOF-MS analysis, where 225 spectra were collected and processed as mentioned above.

To evaluate the impact of signal-to-noise (S/N) threshold on the detection of low-abundance peptide peaks, the data was processed and analysed using a S/N cutoff of 5 as well as 10. While the lower threshold (i.e. S/N= 5) yielded generally good reproducibility (Figure S8). However, to minimise the influence of noise particularly for low-intensity signals near the detection limit, where the blank peaks present as shown in (Figure S9), a higher threshold (i.e. S/N = 10) was selected for the data analysis. After data pre-processing and filtering, only 187 spectra remained. F. nucleatum spectral data was the most affected, which reduced from 25 to just 4, collected from three distinct biological replicates. All of the analysed periodontal bacteria displayed signals in the m/z range between 2000 to 17000, except for P. micra and S. constellatus, which had limited m/z ranges up to ~ 7000 and ~ 9000, respectively. Among the MS spectra of Streptococcus spp., only S. oralis had a significant peak at $\sim 11000 \, m/z$ (Figure S10). The PC-DFA scores plot of the whole m/z range (2000-17000) using 6 PCs (**Figure 2A**), with a TEV of 89.07%, was comparable to the IR findings (Figure 1A), where scree plots were used to select the number of the included PCs (Figure S11). A. israelii was separated from the other samples dominating the negative side of DF1, whereas F. nucleatum and S. oralis were clustered on the negative side of DF2 (Figure **2A**, **2B**, and **2C**). According to DF1 loadings, m/z of 2016 and 2219 were found as the two significant variables that influenced the separation of A. israelii. However, twelve m/z values, including 4626, 5435, 5842, 6157, 6523, 8264, 8688, 9149, 9759, 10460, 11218, and 12388 m/z, were associated with the clustering pattern of F. nucleatum and S. oralis along DF2 (**Table S4**). To further investigate the variance between the strains, we restricted the data only to the higher m/z window of 8000 to 16500, and subjected this to PC-DFA using 6 PCs, with a total explained variance of 83.93% (Figure 2D, E, and F). Using this new range of data, P. gingivalis displayed a clear separation from the other strains according to DF1 axis, which is in agreement with the IR results. Since this clustering pattern was not seen when the whole range was analysed, it indicates the importance of this region for identifying P. gingivalis from the remaining strains. Three m/zvalues at 9329, 9800, and 11029, were found influencing the clustering of P. gingivalis at the higher m/z range. Moreover, eight m/z values including 8256, 8683, 8815, 8908, 9150, 9150, 10459, 11210, and 12389 could be linked to the clustering pattern of S. oralis on the positive side of DF2.

Ribosomal proteins are the most frequently detected proteins in the bacterial MALDI fingerprint because of their widespread distribution inside the bacterial cell and in high abundance (52). These proteins remain unaffected by the phenotypic changes during cultivation, enhancing the reproducibility of MALDI as a technique suitable for clinical laboratory applications (37). The conserved nature of ribosomal protein sequences at the genus level, sometimes even at the species level, allows MALDI to readily detect small variations, enabling differentiation between closely related microorganisms (40). The mass range of 2000 to 20000 *m/z* has been previously reported

as being associated with ribosomal proteins, with few housekeeping proteins and is frequently included on the species level (53, 54). Thus, the *m/z* values highlighted above could be attributed to ribosomal proteins and could be considered for use in organism-specific databases in MALDI-MS profiling.

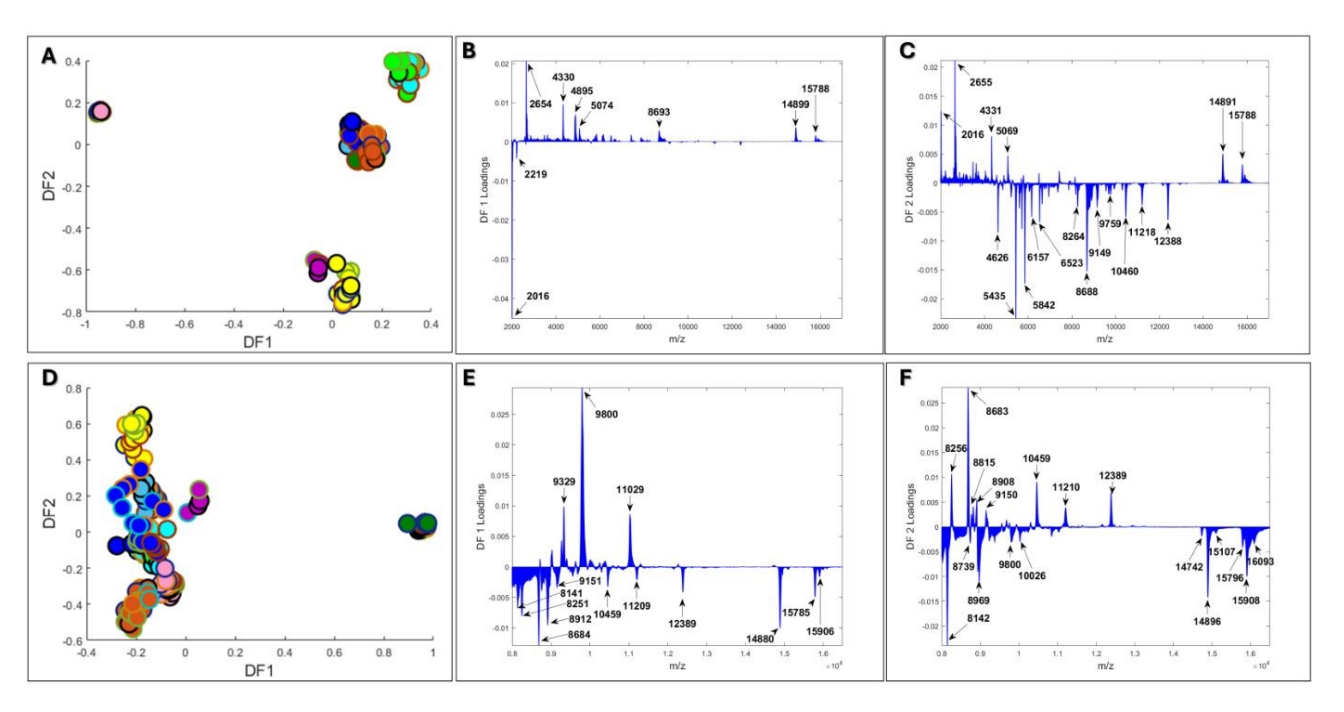


Figure 2 (A) shows PC-DFA scores plot of the complete MALDI-TOF-MS mass spectral data (2000-17000 m/z), using 6 PCs (TEV= 89.07%), while (B) and (C) represent DF1, and DF2 loadings plot associated with the full range. However, (D) shows PC-DFA score plot of the limited high range (8000-16500 m/z) using 4 PCs (TEV= 83.93%), whereas (E), and (F) represent DF1, and DF2 loadings at this range, respectively. All the significant loadings are presented at (Table S2). In (A) and (D), different outline colours were used to represent different biological replicates as each biological replicate was introduced as a separate class (total number of classes 45). Key colours used in figures: S. anginosus (♠), S. constellatus (♠), S. gordonii (♠), S. oralis (♠), S. sanguinis (♠), P. micra (♠), A. israelii (♠), F. nucleatum (♠), and P. gingivalis (♠).

Discrimination at single-cell level

O-PTIR fingerprint analysis

Unlike FT-IR spectra, the O-PTIR spectra displayed a lower signal-to-noise ratio. This is of course as expected, as the O-PTIR analysis was carried out on single bacterial cells where the amount of biomass being analysed is significantly lower, around 1 pg of material. Therefore, following the filtration step outlined in the methods section, approximately five to eight spectral data points were obtained for each strain. (**Figure S12**). While the clustering pattern of PCA score plot, with combined total explained variance of 74.75% within the dataset (**Figure 3A**), is not as distinct as that observed in the FT-IR data, it remains comparable to patterns obtained from the FT-IR analysis (**Figure 1A**). *P. gingivalis* and *F. nucleatum* along with *S. oralis* separated on the negative side of PC1 influenced by vibrational bands at 1353 cm⁻¹ and 1411 cm⁻¹, which are attributed to C=O symmetric stretching of COO- group in amino acids and fatty acids, in addition to N-H bending coupled with C-N stretching at amide II absorption band at 1551 cm⁻¹ and C=O stretching at amide I band at 1655 cm⁻¹ (**Figure 3B**). Due to the higher spatial resolution of O-PTIR, this

47 48

49

50

51 52

53

54

55 56

57

58

59 60 technique can detect within population heterogeneity, which likely contributes to the broad article online spread of clusters and the less distinct separation compared to FT-IR. The observed heterogeneity within the community, captured by O-PTIR, may also explain why *F. nucleatum* clusters in a different region and appears less reproducible than in the FT-IR data. Importantly, the vibrational bands corresponding to N–H bending coupled with C–N stretching at the amide II absorption band (1551 cm⁻¹) and C=O stretching at the amide I band (1655 cm⁻¹) were found to be in agreement with the FT-IR results, while the vibrational bands at 1353 cm⁻¹ and 1411 cm⁻¹ are not present in the FT-IR PCA loadings, however, we consider it important to note their presence alongside the aforementioned amide bands in O-PTIR PC-loadings, as they could be attributed single-cell variability contributing to the overall clustering pattern.

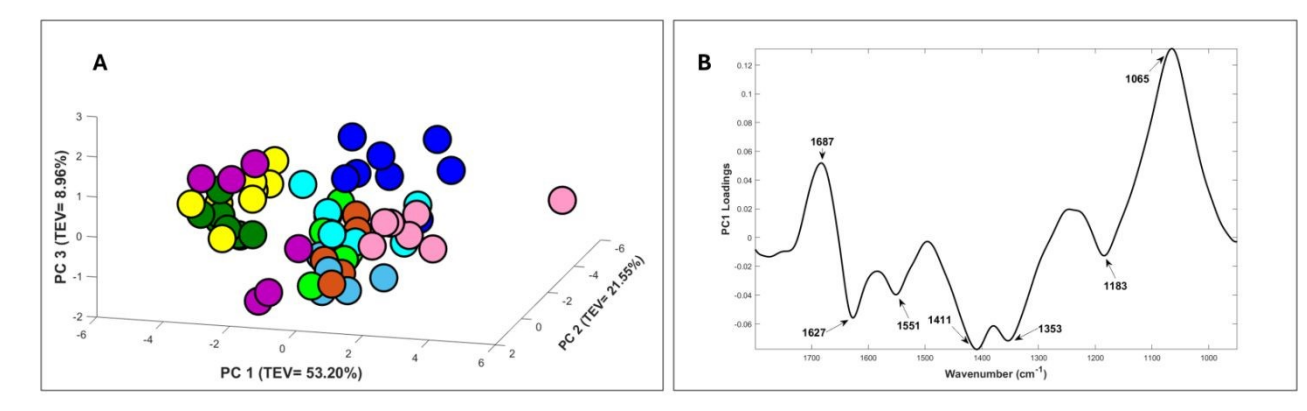


Figure 3 (**A**) shows PCA score plot of the processed O-PTIR spectral data of the nine periodontal bacteria at single-cell level within the fingerprint region (950-1800 cm⁻¹) as multiple principle components were plotted PC1 vs. PC2 vs. PC3, where different colours represent different species. Key colours used in figures: *S. anginosus* (•), *S. constellatus* (•), *S. gordonii* (•), *S. oralis* (•), *S. sanguinis* (•), *P. micra* (•), *A. israelii* (•), *F. nucleatum* (•), and *P. gingivalis* (•). (**B**) represents the PC1 loadings plot, which accounts for the maximum variance in the dataset including fingerprint region (950-1800 cm⁻¹).

Recent studies have demonstrated the lower reproducibility of O-PTIR clustering patterns compared to FT-IR findings (18, 34) In FT-IR, the spectral data represent an averaged signal from the microbial community of each sample, as it captures a larger area with lower spatial resolution. In contrast, the higher spatial resolution of the O-PTIR technique enables the detection of heterogeneity between individual cells, preserving important insights that would be lost when averaging the response from a broader bacterial community. To investigate further the metabolic fingerprints at the bulk and single-cell levels, the relative ratios of the key vibrational features contributing to the clustering patterns observed by FT-IR and O-PTIR using baseline corrected data were compared (**Figure 4**). FT-IR relative ratios of peak intensities of proteins (1654 cm⁻¹), lipid esters (1740 cm⁻¹), and fatty acids (2920 cm⁻¹), to polysaccharides (1061 cm⁻¹) were calculated and presented as box whisker plots (**Figure 4A-C**). These findings suggested that P. gingivalis and F. nucleatum have the highest protein and lipid to polysaccharide ratios when compared to the other strains. At the single-cell level, the O-PTIR findings also displayed similar trends, where the relative ratios of protein (1655 cm⁻¹) to polysaccharide (1063 cm⁻¹) intensities indicated that P. gingivalis, F. nucleatum, and S. oralis have the highest protein to polysaccharide ratios (**Figure 4D**). This is perhaps not surprising as both *P. gingivalis* and *F. nucleatum* are Gramnegative anaerobes, and the high ratios of protein and lipid could be attributed to the nature of the structure of the Gram-negative bacterial cells when compared with Gram-positive ones.

However, the capabilities of our current O-PTIR setup are limited to measuring infrared specific Online exclusively within the fingerprint region (950–1800 cm⁻¹), due to constraints imposed by the instrument setup and the spectral range of the QCL, which selectively covers this region (Lima et al., 2022). As a result, lipid ratios at the single-cell level were calculated only using the peak intensity of the lipid ester vibrational band at 1740 cm⁻¹, with *P. gingivalis* exhibiting the highest relative ratio (**Figure 4E**).

Next, we utilised the targeted single-frequency imaging capabilities of the O-PTIR setup to image the bacterial cells. These single-frequency photothermal images serve as label-free biochemical maps, acquired in a contactless manner. By tuning the laser to specific vibrational bands, the images reveal the relative cellular distribution of key biomolecules such as proteins, lipids, and polysaccharides. The results of O-PTIR images collected at amide I (1655 cm⁻¹) and polysaccharides (1061 cm⁻¹) vibrational bands (**Figure 5**) were in agreement with the calculated relative ratio results. Variation of protein content between periodontal bacteria can be seen across the images that were collected. Although both *P. gingivalis* and *F. nucleatum* displayed the highest protein content as previously determined by the relative ratio calculations, the coccobacillus morphological nature of *P. gingivalis* makes its protein content less visually prominent in comparison to the spindle-shaped cells of *F. nucleatum*.

Pen Access Article Dublished on 42 November 4025, Downhoaded on 44. N. 2025 17:55: 19.

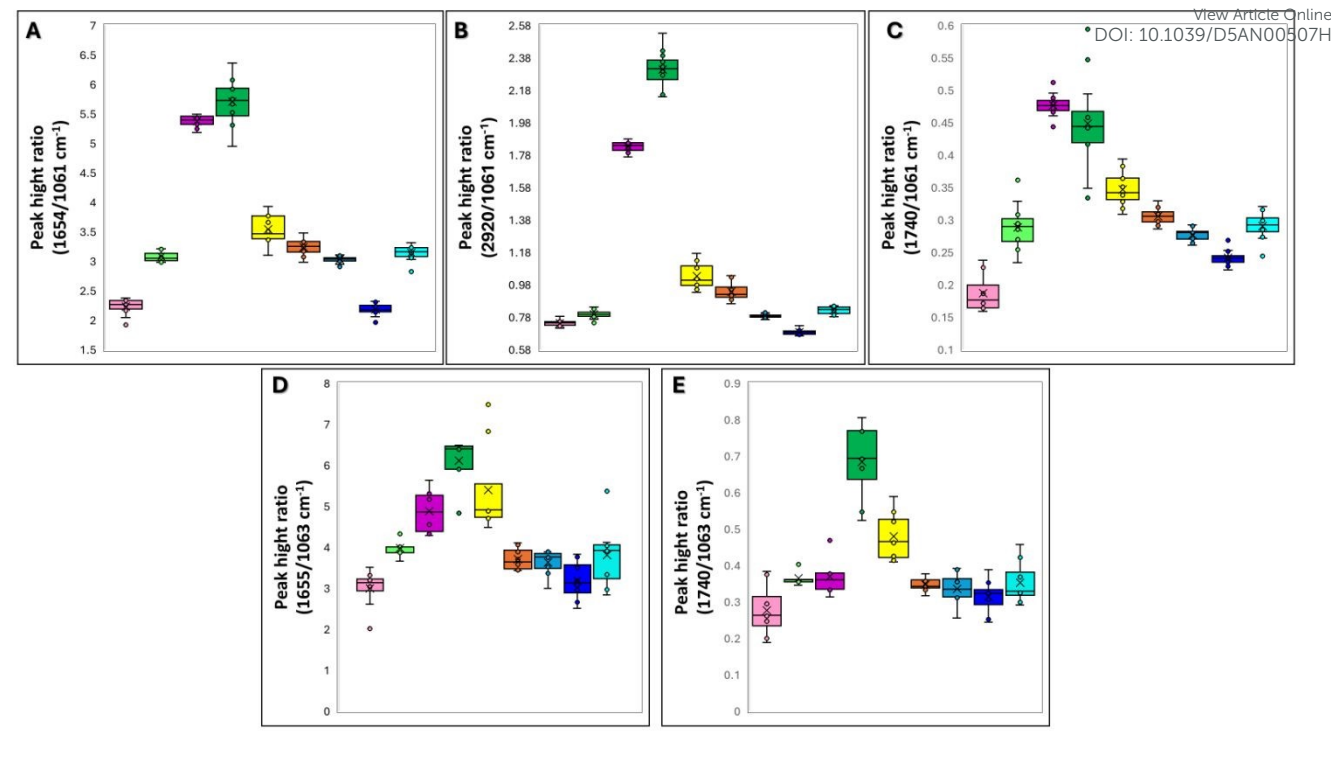


Figure 4 represents the calculated relative ratios of bacterial cell biomolecules as (A), (B), and (C) show Box whisker plot using FT-IR spectral data, (A) shows the relative ratio of proteins at amide I (C=O stretching at 1654 cm⁻¹) to polysaccharides (C-O stretching at 1061 cm⁻¹). (B) and (C) represent relative ratios of lipids at (CH2 asymmetric stretching at 2029 cm⁻¹), and lipid esters (C=O stretching at 1740 cm⁻¹), respectively, to polysaccharides vibrational band at 1061 cm⁻¹. However, (D) and (E) show Box whisker plot using O-PTIR spectral data. (D) and (E) plots respectively show the relative ratio of proteins at amide I (C=O stretching at 1655 cm⁻¹), and lipid esters (C=O stretching at 1740 cm⁻¹) to polysaccharides (C-O stretching at 1061 cm⁻¹) to compare the variances in the relative cellular content of proteins, lipids, and polysaccharides at single-cell level. Key colours used in figures: *S. anginosus* (•), *S. constellatus* (•), *S. gordonii* (•), *S. oralis* (•), *S. sanguinis* (•), *P. micra* (•), *A. israelii* (•), *F. nucleatum* (•), and *P. gingivalis* (•).

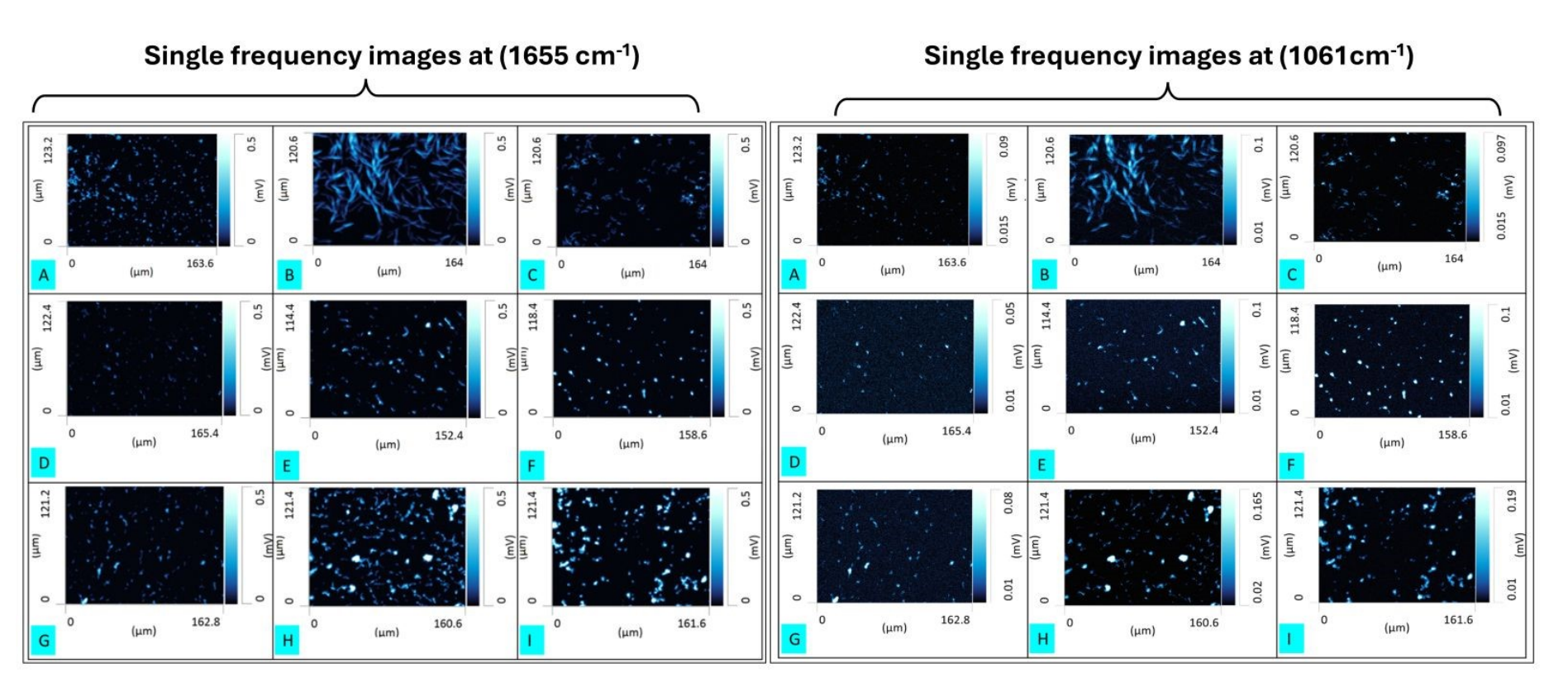


Figure 5 Single-frequency O-PTIR images using amide I vibration at 1655 and polysaccharides vibration at 1061 cm⁻¹ showing the relative concentration of proteins and polysaccharides of periodontal bacteria at single-cell level (**A**) *P. gingivalis*, (**B**) *F. nucleatum*, (**C**) *A. israelii*, (**D**) *P. micra*, (**E**) *S. sanguinis*, (**F**) *S. anginosus*, (**G**) *S. constellatus*, (**H**) *S. gordonii*, and (**I**) *S. oralis*.

60

Furthermore, potential variation of the cellular protein content was assessed by O-PTIR imaging Noo507H at amide I, where higher protein abundance was observed in S. gordonii and S. oralis in comparison to the remaining Streptococcus spp. (Figure 5E-I). However, since the method was applied for qualitative analysis, future study for quantitative image-based evaluation is recommended. Over the years, there have been challenges in accurately identifying oral Streptococcus spp. and categorising them within the phylogenetic microbiota. The oral streptococci involved in this study were recently phylogenomically categorised into discrete groups: S. anginosus and S. constellatus (S. anginosus group - SAG), S. oralis, S. sanguinis and S. gordonii (mitis group) (49, 55). Furthermore, literature has demonstrated challenges in classifying SAG species, leading to limitations in comprehending their role as potential pathogens (56). To investigate these potential variations further, the FT-IR and O-PTIR spectral data of the streptococcal samples were analysed separately. Due to restricted spectral range of the O-PTIR data, the FT-IR data was also limited to the region of (950 - 1800 cm⁻¹) to allow for a fair comparative analysis. The PCA scores plot of FT-IR and O-PTIR data, using this limited range, accounting for combined total explained variance 80.7 and 67.29%, respectively (Figure 6), displayed clear separation of S. anginosus and S. oralis from all other streptococcal strains. In the PC-DFA score plot of the FT-IR spectral data (Figure 6A), S. anginosus was clustered on the positive side of PC1, while S. oralis was clustered on the negative side, while displaying separate clusters compared with regard to other streptococci, according to PC2 axis. According to PCA loadings plot (Figure 6B, and 6C), vibrational bands at 1066 cm⁻¹ and 1123 cm⁻¹ influence the separation of S. anginosus on the positive side of PC1, while vibrational bands at 1697 cm⁻¹, 1624 cm⁻¹, 1523 cm⁻¹, and 1491 cm⁻¹ are the main contributors to the separation of S. oralis from the remaining streptococci. Similarly, for O-PTIR, S. anginosus and S. oralis were separated from other strains on the negative side of PC1 axis (Figure 6D). However, both were clearly separated from one another based on PC2 axis. According to PC1 and PC2 loadings, the vibrational bands that influenced their separation were found aligned with the FT-IR findings. The trends observed by both IR-based methods displayed comparable results, with S. anginosus showing the lowest lipids to polysaccharides ratio, whereas S. oralis presented the highest ratio. In addition, according to both, FT-IR and O-PTIR findings, S. oralis exhibited the highest relative ratio of protein to polysaccharide among the streptococcal species, while S. anginosus exhibited the lowest ratio. These findings are consistent with our MALDI-MS results (Figure 2), where S. oralis clustered separately from the other streptococcal samples and exhibited a notably richer MALDI-MS spectral profile (Figure S10H). It noteworthy that the clustering pattern observed is consistent with the findings of a previous FT-IR analysis of oral streptococci conducted by Van der Mei et.al., in which S. sanguinis and S. gordonii where grouped together alongside three isolates of S. mitis (57).

4

5 6 7

8

9

10 11

12 13 14

Pen Access Article, Published on 42 November 4025, Downhoad on 44. N. 2025 L7:55: U. L. Article II. Rense Linder & Creative Commons Attribution 5:0 On ported Liberice.

45

46 47

48

49

50 51

52

53

54 55

56

57

58 59

60

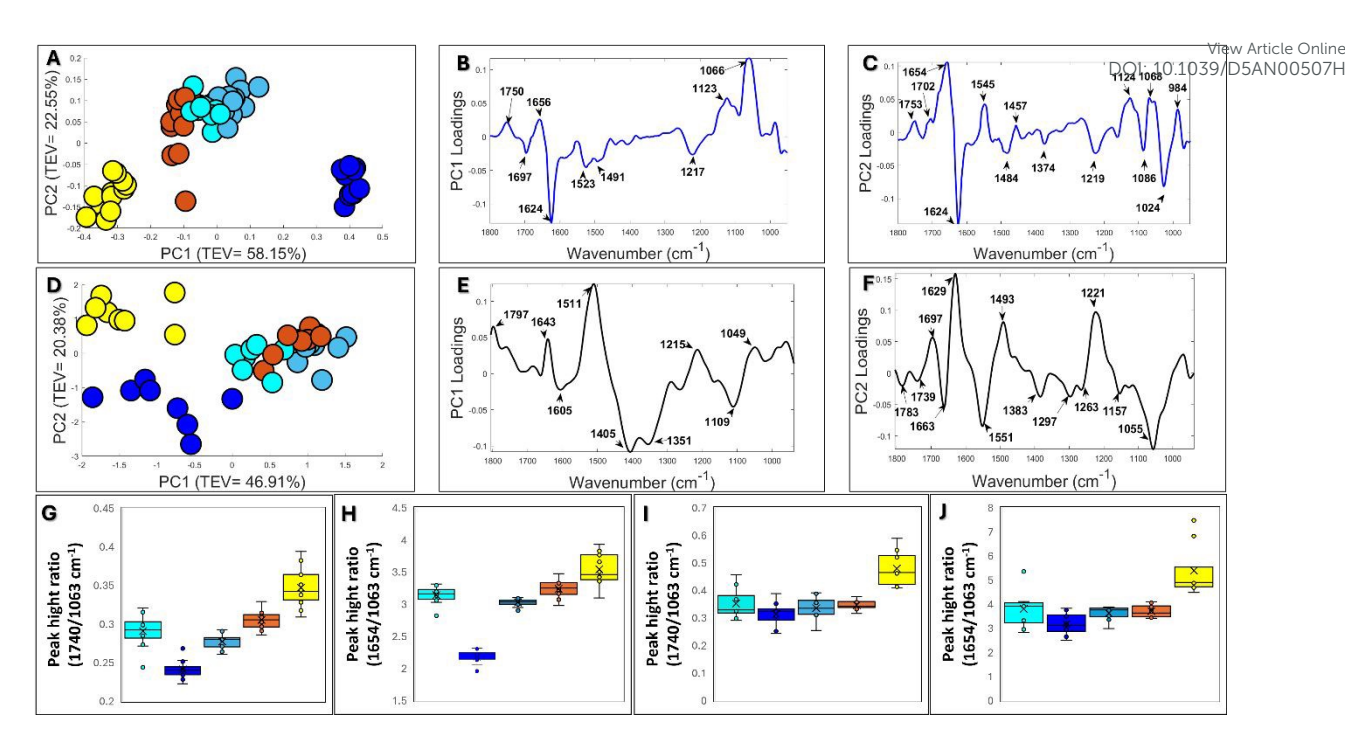


Figure 6 Comparative discrimination of streptococcal strains using the vibrational spectroscopy techniques data. (A) represent PCA score plot of the processed FT-IR data using fingerprint region (950-1800 cm⁻¹), while (B) and (C) show PC1 and PC2 loadings plots, respectively. However, (D) represent PCA score plot of the processed O-PTIR data using fingerprint region (950-1800 cm⁻¹, while (E) and (F) show PC1 and PC2 loadings, respectively. (G), and (H) show Box whisker plot of FT-IR spectral raw data. (G), and (H) plots respectively show the relative ratio of lipid esters (C=O stretching at 1740 cm⁻¹), and proteins at amide I (C=O stretching at 1654 cm⁻¹) to polysaccharides (C-O stretching at 1061 cm⁻¹) highlighting the variances in the cellular content of proteins, lipids, and polysaccharides at microbial community level (FT-IR data). However, (I) and (J) plots show the variance of the relative ratio of proteins, and lipid esters, respectively, to polysaccharides at single-cell level (O-PTIR data). Key colours used in figures: S. anginosus (•), S. constellatus (•), S. gordonii (•), S. oralis (•), and S. sanguinis (•).

Biochemical profiling through employing traditional and advanced analytical techniques has been widely utilised in microbial identification and classification, providing insights into metabolic capabilities and phenotypic traits. To the best of our knowledge, IR-based findings in this study highlighted the biochemical diversity among periodontal bacteria, aligning with literature reports on their distinct cellular compositions. The observed spectral variations and classification patterns reflect key differences in macromolecular content, including proteins, lipids, and polysaccharides, which underpin species-specific metabolic adaptations and functional roles within the periodontal microbiome. However, since FT-IR spectroscopy provides information primarily about functional groups rather than specific molecular identities, it remains challenging to assign the exact biomolecules responsible for the observed clustering. This highlights a gap in the current understanding and emphasising the need for complementary techniques to achieve a more precise molecular characterisation. Another limitation of this study is the nature of O-PTIR measurements requiring manual data collection, which is in fact poses practical limitations. In our study, this resulted in the acquisition of data from only 55 cells, and due to the low signal-to-noise ratio, we were able to include only eight individual cells per species. Nevertheless, within this dataset, we can clearly observe heterogeneity within the community, as exemplified by F. nucleatum. In contrast, this heterogeneity is not apparent in the FT-IR results, as the larger beam size averages out these intra-population variations. However, given the high spatial resolution of O-PTIR, future studies should include a larger number of individual cells to better account for intra-species

4

5

6 7

8

9

10 11

12

13

14

Pen Access Article, Published on 12 November 1025, Downhoaded on 14. N. 2025 L7:55: LD ... Answerige and Physical Conference of Creative Commons. Sturbution 5:0 Unported Liberson

45

46

47 48

49

50 51

52 53

54

55

56

57 58

59

60

heterogeneity. On the other hand, the single-cell sensitivity demonstrated by O-PTIR suggesticle Online promising potential for direct application to clinical samples, such as saliva. As it has been previously described by Barros et al, chronic periodontitis is associated with increased permeability of the junctional epithelium and a significant rise in gingival crevicular fluid (GCF) flow rate (58). GCF leakage into saliva makes it a valuable target for the detection of the subgingival pathogens (5). Such bacteria are known for their fastidious nature and typically require prolonged culturing, which complicates traditional detection methods. By enabling biochemical profiling without extensive cultivation, O-PTIR could significantly enhance the rapid detection of such pathogens. However, further method optimisation is needed to address the complexity of the clinical samples, including minimising background interference and distinguishing between multiple bacterial species within mixed populations. With these advancements, O-PTIR could become a powerful tool for rapid and less invasive clinical diagnostics.

Conclusion

This study explored the biochemical composition differences among nine periodontal bacteria including P. gingivalis, S. anginosus, S. constellatus, S. gordonii, S. sanguinis, S. oralis, A. israelii, F. nucleatum, and P. micra, which are representatives of the subgingival plaque complexes. Combined with chemometrics, they were analysed at the microbial-community level using FT-IR spectroscopy, and MALID-TOF-MS to allow for classification and differentiation of these clinically significant species. To investigate the heterogenicity between single cells within the community, and explore the tantalising potential of bypassing the prolonged culturing requirements of some of these anaerobic microorganisms, O-PTIR spectroscopy was also employed. The findings displayed substantial variations in biochemical composition across the strains studied, with three exhibiting notably higher ratios of protein and lipid to polysaccharides than the remaining strains P. gingivalis, F. nucleatum, and S. oralis, while S. anginosus demonstrated the lowest observed ratio. IR clustering patterns were found comparable to MALDI-MS results. Furthermore, according to MALID-MS, around 20 m/z values were found influencing the classification pattern of A. israelii, P. gingivalis, F. nucleatum, and S. oralis, increasing the potential of using the defined m/z values as biomarkers for their identification. Such results suggest future research to identify the molecular constituents underlying the observed m/z values. It is recommended to employ methods that could offer deeper insights into the variability of protein and lipid profiles among these bacteria, such as using liquid chromatography mass spectrometry (LC-MS) for lipid profiling and proteomic pipelines for protein analysis. Overall, this study advances our understanding of the biochemical diversity present in periodontitisassociated bacteria and broadens the analytical approaches available for future research on their pathogenicity, which may guide future targeted therapeutic strategies.

Author Contributions

JA: experimental design, sample collection and preparation, MALDI, FT-IR and O-PTIR data analysis, data interpretation, and manuscript writing; DS: O-PTIR data collection; SR: MALDI training and instrument automation; YX: assistance with MALDI data analysis; HA and KAW: data interpretation, and manuscript preparation; HM: principal investigator, experimental design, data interpretation, and manuscript preparation. All authors reviewed and approved the final manuscript.

Analyst Accepted Manuscrip

58

59

60

View Article Online Acknowledgments DOI: 10.1039/D5AN00507H

HM would like to thank the University of Liverpool, and Analytical Chemistry Trust Fund (ACTF) and Community for Analytical Measurement Science (CAMS) for funding and support (600310/22/09). JA was funded by a PhD scholarship from King Khalid University, Kingdom of Saudi Arabia. MALDI-TOF-MS work made use of shared equipment located at the Materials Innovation Factory, created as part of the UK Research Partnership Innovation Fund (Research England) and co-funded by the Sir Henry Royce Institute. We would like to acknowledge Roy Goodacre, Najla AlMasoud, and members of Centre of Metabolomics Research for their valuable advice throughout this work.

Data Availability

All data generated in this study will be made available upon request.

Conflicts of Interest

The authors declare that they have no competing interests.

References

- Caranza FA, Newman MG, Glickman's I. Clinical periodontology. Philadelphia, 1996—470p. 1. 1996.
- Tonetti MS, Greenwell H, Kornman KS. Staging and grading of periodontitis: Framework and 2. proposal of a new classification and case definition. J Periodontol. 2018;89 Suppl 1:S159-S72.
- Socransky SS, Haffajee AD, Cugini MA, Smith C, Kent RL. Microbial complexes in subgingival plaque. J Clin Periodontol. 1998;25(2):134-44.
- da Silva-Boghossian CM, do Souto RM, Luiz RR, Colombo APV. Association of red complex, A. actinomycetemcomitans and non-oral bacteria with periodontal diseases. Archives of Oral Biology. 2011;56(9):899-906.
- Albahri J, Allison H, Whitehead KA, Muhamadali H. The role of salivary metabolomics in chronic periodontitis: bridging oral and systemic diseases. Metabolomics. 2025;21(1):24.
- Gaur S, Agnihotri R. A lzheimer's disease and chronic periodontitis: Is there an association? Geriatrics & gerontology international. 2015;15(4):391-404.
- 7. Olsen I, Kell DB, Pretorius E. Is Porphyromonas gingivalis involved in Parkinson's disease? Eur J Clin Microbiol Infect Dis. 2020;39(11):2013-8.
- Lapo S, Leonardo C, Luigi B, Michele N, Sergio S, Calogero Lino C, et al. Association between 8. chronic kidney disease and periodontitis. A systematic review and metanalysis. Oral Diseases. 2021.
- Chapple IL, Genco R, workshop WgojEA. Diabetes and periodontal diseases: consensus report of the Joint EFP/AAP Workshop on Periodontitis and Systemic Diseases. J Clin Periodontol. 2013;40 Suppl 14:S106-12.
- Botelho J, Machado V, Leira Y, Proença L, Chambrone L, Mendes JJ. Economic burden of periodontitis in the United States and Europe: An updated estimation. J Periodontol. 2022;93(3):373-9.
- Sedghi L, DiMassa V, Harrington A, Lynch SV, Kapila YL. The oral microbiome: Role of key organisms and complex networks in oral health and disease. Periodontol 2000. 2021;87(1):107-31.
- 12. Abusleme L, Hoare A, Hong BY, Diaz PI. Microbial signatures of health, gingivitis, and periodontitis. Periodontol 2000. 2021;86(1):57-78.
- Arbefeville SS, Timbrook TT, Garner CD. Evolving strategies in microbe identification-a comprehensive review of biochemical, MALDI-TOF MS and molecular testing methods, J Antimicrob Chemother. 2024;79(Supplement 1):i2-i8.
- Gajic I, Kabic J, Kekic D, Jovicevic M, Milenkovic M, Mitic Culafic D, et al. Antimicrobial Susceptibility Testing: A Comprehensive Review of Currently Used Methods. Antibiotics (Basel). 2022;11(4).

4

5

6

7

8

9

10

11

12

13

14

15

Pen Access the right of reduction 12 November 1024, Downbarded on 14: 14, 2025 17:55: ID.
This afficiers Received a Creative Commons. Kirrbuton 5:0 Ongored 19e

45

46

47

48

49

50

51

52

53

54

55

56

57

58

59

60

- 15. Movasaghi Z, Rehman S, ur Rehman DI. Fourier Transform Infrared (FTIR) Spectroscopy Agree Online Biological Tissues. Applied Spectroscopy Reviews. 2008;43(2):134-79.
- 16. Wenning M, Scherer S. Identification of microorganisms by FTIR spectroscopy: perspectives and limitations of the method. Appl Microbiol Biotechnol. 2013;97(16):7111-20.
- 17. Ahmed S, Albahri J, Shams S, Sosa-Portugal S, Lima C, Xu Y, et al. Rapid Classification and Differentiation of Sepsis-Related Pathogens Using FT-IR Spectroscopy. Microorganisms. 2024;12(7).
- 18. Lima C, Muhamadali H, Goodacre R. Simultaneous Raman and Infrared Spectroscopy of Stable Isotope Labelled. Sensors (Basel). 2022;22(10).
- 19. Helm D, Labischinski H, Schallehn G, Naumann D. Classification and identification of bacteria by Fourier-transform infrared spectroscopy. J Gen Microbiol. 1991;137(1):69-79.
- 20. Mohamed MA, Jaafar J, Ismail AF, Othman MHD, Rahman MA. Chapter 1 Fourier Transform Infrared (FTIR) Spectroscopy. In: Hilal N, Ismail AF, Matsuura T, Oatley-Radcliffe D, editors. Membrane Characterization: Elsevier; 2017. p. 3-29.
- 21. Enders AA, North NM, Fensore CM, Velez-Alvarez J, Allen HC. Functional Group Identification for FTIR Spectra Using Image-Based Machine Learning Models. Analytical Chemistry. 2021;93(28):9711-8.
- 22. Zhang X, Yang F, Xiao J, Qu H, Jocelin NF, Ren L, et al. Analysis and comparison of machine learning methods for species identification utilizing ATR-FTIR spectroscopy. Spectrochimica Acta Part A: Molecular and Biomolecular Spectroscopy. 2024;308:123713.
- 23. El Orche A, Cheikh A, Johnson JB, Elhamdaoui O, Jawhari S, El Abbes FM, et al. A Novel Approach for Therapeutic Drug Monitoring of Valproic Acid Using FT-IR Spectroscopy and Nonlinear Support Vector Regression. J AOAC Int. 2023;106(4):1070-6.
- 24. Ouhaddouch H, Cheikh A, Idrissi MOB, Draoui M, Bouatia M. FT-IR Spectroscopy Applied for Identification of a Mineral Drug Substance in Drug Products: Application to Bentonite. Journal of Spectroscopy. 2019;2019(1):2960845.
- 25. Finlayson D, Rinaldi C, Baker MJ. Is Infrared Spectroscopy Ready for the Clinic? Anal Chem. 2019;91(19):12117-28.
- 26. Yang B, Chen C, Chen C, Cheng H, Yan Z, Chen F, et al. Detection of breast cancer of various clinical stages based on serum FT-IR spectroscopy combined with multiple algorithms. Photodiagnosis and Photodynamic Therapy. 2021;33:102199.
- 27. Badawi A, Althobaiti MG. Effect of Cu-doping on the structure, FT-IR and optical properties of Titania for environmental-friendly applications. Ceramics International. 2021;47(8):11777-85.
- 28. Della Ventura G, Bellatreccia F, Marcelli A, Cestelli Guidi M, Piccinini M, Cavallo A, et al. Application of micro-FTIR imaging in the Earth sciences. Anal Bioanal Chem. 2010;397(6):2039-49.
- 29. Reffner J. Advances in infrared microspectroscopy and mapping molecular chemical composition at submicrometer spatial resolution. Spectroscopy. 2018;33(9):12–7--7.
- 30. Xu J, Li X, Guo Z, Huang WE, Cheng JX. Fingerprinting Bacterial Metabolic Response to Erythromycin by Raman-Integrated Mid-Infrared Photothermal Microscopy. Anal Chem. 2020;92(21):14459-65.
- 31. Klementieva O, Sandt C, Martinsson I, Kansiz M, Gouras GK, Borondics F. Super-Resolution Infrared Imaging of Polymorphic Amyloid Aggregates Directly in Neurons. Adv Sci (Weinh). 2020;7(6):1903004.
- 32. Kansiz M, Dowling LM, Yousef I, Guaitella O, Borondics F, Sulé-Suso J. Optical Photothermal Infrared Microspectroscopy Discriminates for the First Time Different Types of Lung Cells on Histopathology Glass Slides. Anal Chem. 2021;93(32):11081-8.
- 33. Lima C, Muhamadali H, Xu Y, Kansiz M, Goodacre R. Imaging Isotopically Labeled Bacteria at the Single-Cell Level Using High-Resolution Optical Infrared Photothermal Spectroscopy. Anal Chem. 2021;93(6):3082-8.
- 34. Shams S, Lima C, Xu Y, Ahmed S, Goodacre R, Muhamadali H. Optical photothermal infrared spectroscopy: A novel solution for rapid identification of antimicrobial resistance at the single-cell level. Front Microbiol. 2023;14:1077106.
- 35. Spadea A, Denbigh J, Lawrence MJ, Kansiz M, Gardner P. Analysis of Fixed and Live Single Cells Using Optical Photothermal Infrared with Concomitant Raman Spectroscopy. Anal Chem. 2021;93(8):3938-50.

Analyst Accepted Manuscript

58

59

60

- Muhamadali H, Weaver D, Subaihi A, AlMasoud N, Trivedi DK, Ellis DI, et al. Chickenticle Online 36. beams, and Campylobacter: rapid differentiation of foodborne bacteria via vibrational spectroscopy and MALDI-mass spectrometry. Analyst. 2016;141(1):111-22.
- AlMasoud N, Muhamadali H, Chisanga M, AlRabiah H, Lima CA, Goodacre R. Discrimination of bacteria using whole organism fingerprinting: the utility of modern physicochemical techniques for bacterial typing. Analyst. 2021;146(3):770-88.
- Fuchs B, Süss R, Schiller J. An update of MALDI-TOF mass spectrometry in lipid research. Prog Lipid Res. 2010;49(4):450-75.
- 39. Sauer S, Kliem M. Mass spectrometry tools for the classification and identification of bacteria. Nat Rev Microbiol. 2010;8(1):74-82.
- Clark AE, Kaleta EJ, Arora A, Wolk DM. Matrix-assisted laser desorption ionization-time of flight mass spectrometry: a fundamental shift in the routine practice of clinical microbiology. Clin Microbiol Rev. 2013;26(3):547-603.
- Stîngu CS, Rodloff AC, Jentsch H, Schaumann R, Eschrich K. Rapid identification of oral anaerobic bacteria cultivated from subgingival biofilm by MALDI-TOF-MS. Oral Microbiol Immunol. 2008;23(5):372-6.
- 42. Muhamadali H, Xu Y, Morra R, Trivedi DK, Rattray NJ, Dixon N, et al. Metabolomic analysis of riboswitch containing E. coli recombinant expression system. Mol Biosyst. 2016;12(2):350-61.
- Tengsuttiwat T, Kaderbhai NN, Gallagher J, Goodacre R, Muhamadali H. Metabolic Fingerprint Analysis of Cytochrome. Front Microbiol. 2022;13:874247.
- Martens H, Nielsen JP, Engelsen SB. Light scattering and light absorbance separated by extended multiplicative signal correction. application to near-infrared transmission analysis of powder mixtures. Anal Chem. 2003;75(3):394-404.
- Gross JH. Mass Spectrometry: A Textbook. 2nd ed. Berlin, Heidelberg: Springer Nature; 2006. 45.
- 46. Parker KC. Scoring methods in MALDI peptide mass fingerprinting: ChemScore, and the ChemApplex program. Journal of the American Society for Mass Spectrometry. 2002;13(1):22-39.
- 47. Hotelling H. Analysis of a complex of statistical variables into principal components. Journal of educational psychology. 1933;24(6):417.
- Gromski PS, Muhamadali H, Ellis DI, Xu Y, Correa E, Turner ML, et al. A tutorial review: 48. Metabolomics and partial least squares-discriminant analysis--a marriage of convenience or a shotgun wedding. Anal Chim Acta. 2015;879:10-23.
- Imai K, Nemoto R, Kodana M, Tarumoto N, Sakai J, Kawamura T, et al. Rapid and Accurate Species Identification of Mitis Group Streptococci Using the MinION Nanopore Sequencer. Front Cell Infect Microbiol. 2020;10:11.
- Zheng W, Tan TK, Paterson IC, Mutha NV, Siow CC, Tan SY, et al. StreptoBase: An Oral Resource and Analysis Platform. PLoS Streptococcus mitis Group Genomic 2016;11(5):e0151908.
- 51. McGalliard R, Muhamadali H, AlMasoud N, Haldenby S, Romero-Soriano V, Allman E, et al. Bacterial discrimination by Fourier transform infrared spectroscopy, MALDI-mass spectrometry and whole-genome sequencing. Future Microbiol. 2024;19(9):795-810.
- Ramakrishnan V, White SW. Ribosomal protein structures: insights into the architecture, 52. machinery and evolution of the ribosome. Trends in Biochemical Sciences. 1998;23(6):208-12.
- Singhal N, Kumar M, Kanaujia PK, Virdi JS. MALDI-TOF mass spectrometry: an emerging technology for microbial identification and diagnosis. Front Microbiol. 2015;6:791.
- 54. Murray PR. What is new in clinical microbiology-microbial identification by MALDI-TOF mass spectrometry: a paper from the 2011 William Beaumont Hospital Symposium on molecular pathology. J Mol Diagn. 2012;14(5):419-23.
- Richards VP, Palmer SR, Pavinski Bitar PD, Qin X, Weinstock GM, Highlander SK, et al. Phylogenomics and the dynamic genome evolution of the genus Streptococcus. Genome Biol Evol. 2014;6(4):741-53.
- Pilarczyk-Zurek M, Sitkiewicz I, Koziel J. The Clinical View on. Front Microbiol. 56. 2022;13:956677.
- van der Mei HC, Naumann D, Busscher HJ. Grouping of oral streptococcal species using fourier-transform infrared spectroscopy in comparison with classical microbiological identification. Archives of Oral Biology. 1993;38(11):1013-9.

58. Barros SP, Williams R, Offenbacher S, Morelli T. Gingival crevicular fluid as a source of the Online biomarkers for periodontitis. Periodontol 2000. 2016;70(1):53-64.

View Article Online DOI: 10.1039/D5AN00507H

Analyst Accepted Manuscript

Data Availability

All data generated in this study will be made available upon request.